9th International Conference on Numerical Ship Hydrodynamics
Ann Arbor, Michigan, USA 5-8 August 2007

Prediction of Cavitating Waterjet Propulsor Performance Using a Boundary Element Method

Spyros A. Kinnas[1], Hanseong Lee[2], Thad J. Michael[3] and Hong Sun[1]
([1]The University of Texas at Austin, [2]FloaTEC LLC,
[3]NSWC Carderock Division)

ABSTRACT

The authors present the extension of a previously developed boundary element method to predict the flow inside waterjet pumps, including the effects of sheet cavitation on the blades. The circumferentially averaged interaction between the rotor and the stator is accounted for in an iterative manner. The method is applied in the case of an actual waterjet pump and comparisons of the predicted and the measured rotor torque are presented.

INTRODUCTION

Due to the demand for high speed vessels, the application of waterjet propulsors on commercial and navy vessels has increased in recent years. Waterjets are the propulsion of choice for high-speed naval ships and fast ferries. Compared to conventional propellers, waterjet propulsors provide several advantages. Waterjet propulsors improve maneuverability, reduce the possibility of cavity occurrence by controlling the flow inside the casing, and reduce the likelihood of damage to the blades by protecting them inside the hull. Nevertheless, like in many other fluid machines, such as water turbines, pumps, and marine propellers, the performance of waterjet propulsion systems is affected by cavitation in many significant ways. The foremost hydrodynamic issue is the thrust-breakdown due to cavitation. This inability to increase thrust is accompanied by noise, vibration, and erosion. The issue is more serious and harder to address in the case of waterjet propulsion systems than in conventional propellers, inasmuch as waterjet propulsion systems have several components such as intake duct, rotor, stator, shaft/hub, and casing. Due to the interactions among the flows around the various components, the flow is more complex and multi-featured. Presently, our capability to predict cavitation and its consequences in waterjet propulsors is seriously limited. Model and occasional full-scale measurements are the means that are most often resorted to.

Numerical methods for the prediction of performance and design of the waterjet rotor and stator components were presented in Taylor et al (1998) and Kerwin et al (2006). These methods were based on inviscid flow methods (vortex-lattice methods) applied on the blades of the rotor or stator, coupled with either Reynolds-Averaged Navier-Stokes (RANS) or Euler equations solvers for the solution of the global flow through the pump.

Chun et al (2002) and Brewton et al (2006) applied RANS methods on the rotor and stator blades, where the interaction between the rotor and the stator was considered in the unsteady sense by the former, and in the circumferentially averaged sense by the latter.

A comprehensive review of issues concerning the prediction of performance and design of waterjets was recently presented by Kerwin (2006).

A boundary element method (named PROPCAV) for the analysis of cavitating open propellers subject to a non-uniform inflow was originally developed at MIT by Fine (1992) and Kinnas & Fine (1992). Since then, the method has been improved considerably by the Ocean Engineering Group at UT Austin, to include mid-chord back and/or face cavitation, modeling of super-cavitating and surface-piercing propellers by Young (2002) and Young & Kinnas (2001, 2003, 2004); unsteady wake alignment and developed tip vortex cavitation by Lee (2002) and Lee & Kinnas (2004, 2005); modelling of cavitating propellers inside tunnels and of cavitating ducted propellers by Lee and Kinnas (2006); application to propeller induced rudder cavitation by Kinnas et al (2007); and more recently

coupling with an integral boundary layer solver by Sun and Kinnas (2006).

In this work we present an extension of our previous work to predict the performance of waterjet propulsors, including the presence of sheet cavitation on the rotor and stator blades. We will only address axial flow pumps subject to uniform upstream inflow at this stage. The interaction between rotor and stator will be time-averaged in a similar way as presented in Taylor et al (1998), Kinnas et al (2002), Kerwin et al (2006), and Brewton et al (2006).

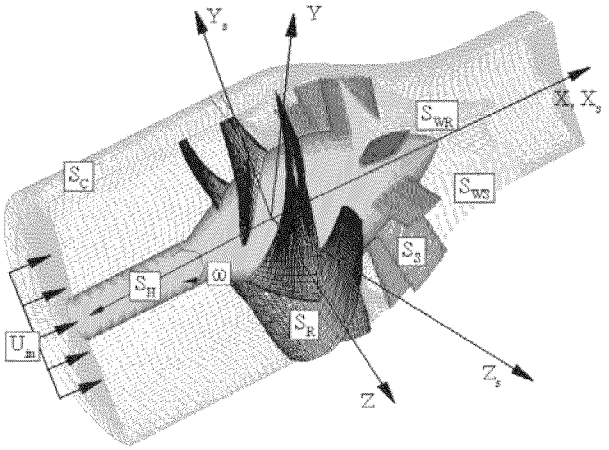

Figure 1: Rotor- and Stator-Fixed Coordinate systems and paneled geometry of waterjet components.

FORMULATION

A waterjet geometry with the related coordinate systems is depicted in Figure 1.

Assumptions

– Inflow at waterjet inlet is uniform ($\vec{U}_{in}$), and defined in the ship fixed coordinate system.
– Waterjet rotor rotates with a constant angular velocity, $\vec{\omega}$.
– Inflow velocity

$\vec{V}_{in}(x,y,z) = \vec{U}_{in}(x,r,\theta)$ in the case of a ship fixed coordinate system

$\vec{V}_{in}(x,y,z) = \vec{U}_{in}(x,r,\theta'-\omega t) - \vec{\omega} \times \vec{x}$ in the case of a rotating coordinate system

– Fluid is inviscid, and the flow is irrotational and incompressible.

$\vec{q}(x,y,z) = \vec{V}_{in}(x,y,z) + \nabla\phi(x,y,z)$

where $\vec{q}(x,y,z)$ is the total velocity, and $\phi(x,y,z)$ is the perturbation potential.

Governing equations and boundary conditions

Integral equation for both rotor and stator: the perturbation potential, $\phi(x,y,z)$, at any point $p(x,y,z)$ located either on the wetted rotor or stator blades and the hub surface, $S_R \cup S_S \cup S_H$, and the casing surface, Sc, or on the cavity surfaces of the rotor or stator, $S_{RC} \cup S_{SC}$, has to satisfy Green's third identity.

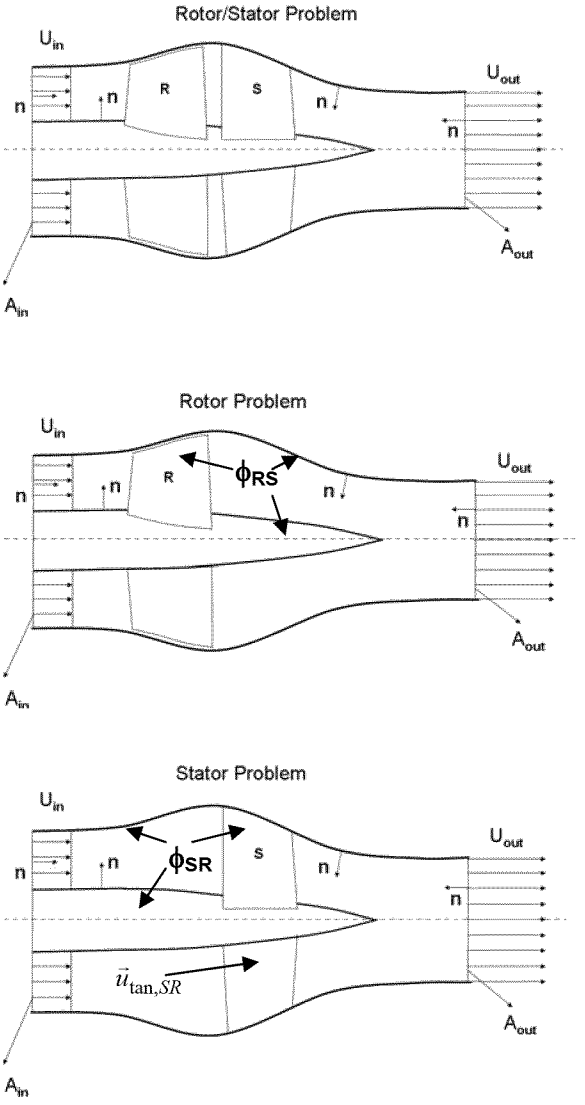

Figure 2: Schematic showing: (a) the combined rotor/stator problem, (b) the rotor problem, and (c) the stator problem. Problems (b) and (c) are solved in sequence with the (time-averaged) effects of one on the other being accounted for in an iterative sense.

$$2\pi\phi(\vec{x}) = \int_{S_R+S_{RC}} \left[\phi_q(\vec{x}) \frac{\partial G(p;q)}{\partial n_q} - G(p;q) \frac{\partial \phi(\vec{x})}{\partial n_q} \right] ds + \int_{S_{RW}} \Delta\phi_{rw}(\vec{x}) \frac{\partial G(p;q)}{\partial n_q} ds + \int_{S_S+S_{SC}} \left[\phi_q(\vec{x}) \frac{\partial G(p;q)}{\partial n_q} - G(p;q) \frac{\partial \phi(\vec{x})}{\partial n_q} \right] ds + \int_{S_{SW}} \Delta\phi_{sw}(\vec{x}) \frac{\partial G(p;q)}{\partial n_q} ds + \int_{S_C} \left[\phi_q(\vec{x}) \frac{\partial G(p;q)}{\partial n_q} - G(p;q) \frac{\partial \phi(\vec{x})}{\partial n_q} \right] ds$$

where the subscripts, q and p, correspond to the variable point and the field point, respectively. $G(p;q) = 1/R(p;q)$ is the Green function, where $R(p;q)$ is the distance between the field point p and the variable point q. $\vec{n}_q$ is the unit normal vector pointing into the flow field. $\Delta\phi_{rw}$ and $\Delta\phi_{sw}$ are the potential jumps in the trailing wake sheets shedding from either the rotor or the stator trailing edge, respectively.

In the above equation, the potentials should also be a function of time, since the interaction between rotor and stator is unsteady in nature. The above equation can be applied with respect to the rotating coordinate system, and in that case the stator is a moving surface and the appropriate kinematic boundary condition must be applied on it, or with respect to the ship-fixed coordinate system, and in that case the rotor is a moving surface. It should be noted that the value of $\frac{\partial \phi}{\partial n}$ for each component is independent of the coordinate system.

In the present approach we will consider the circumferentially averaged effect of each device on the other. In addition we will solve the rotor with respect to the rotating coordinate system and the stator with respect to the fixed coordinates system. The complete rotor/stator, the rotor, and the stator problems are depicted in Figure 2.

Integral equation for waterjet rotor:

$$2\pi\phi(\vec{x}) = \int_{S_R+S_{RC}} \left[\phi_q(\vec{x}) \frac{\partial G(p;q)}{\partial n_q} - G(p;q) \frac{\partial \phi(\vec{x})}{\partial n_q} \right] ds + \int_{S_{RW}} \Delta\phi_{rw}(\vec{x}) \frac{\partial G(p;q)}{\partial n_q} ds + \int_{S_C} \left[\phi_q(\vec{x}) \frac{\partial G(p;q)}{\partial n_q} - G(p;q) \frac{\partial \phi(\vec{x})}{\partial n_q} \right] ds + 4\pi\phi_{RS}(\vec{x})$$

Where $4\pi\phi_{RS}(\vec{x})$ are the circumferentially averaged values of the induced potentials on rotor, hub and waterjet casing due to stator, defined as follows:

$$2\pi\phi_{RS}(\vec{x}) = \int_{S_S+S_{SC}} \left[\phi_q(\vec{x}) \frac{\partial G(p;q)}{\partial n_q} - G(p;q) \frac{\partial \phi(\vec{x})}{\partial n_q} \right] ds + \int_{S_{SW}} \Delta\phi_{sw}(\vec{x}) \frac{\partial G(p;q)}{\partial n_q} ds$$

Integral equation for waterjet stator:

$$2\pi\phi(\vec{x}) = \int_{S_S+S_{SC}} \left[\phi_q(\vec{x}) \frac{\partial G(p;q)}{\partial n_q} - G(p;q) \frac{\partial \phi(\vec{x})}{\partial n_q} \right] ds + \int_{S_{SW}} \Delta\phi_{sw}(\vec{x}) \frac{\partial G(p;q)}{\partial n_q} ds + \int_{S_C} \left[\phi_q(\vec{x}) \frac{\partial G(p;q)}{\partial n_q} - G(p;q) \frac{\partial \phi(\vec{x})}{\partial n_q} \right] ds + 4\pi\phi_{SR}(\vec{x})$$

Where $4\pi\phi_{SR}(\vec{x})$ are the circumferentially averaged values of the induced potentials on the stator, hub and waterjet casing due to the rotor, defined as follows:

$$2\pi\phi_{SR}(\vec{x}) = \int_{S_R+S_{RC}} \left[\phi_q(\vec{x}) \frac{\partial G(p;q)}{\partial n_q} - G(p;q) \frac{\partial \phi(\vec{x})}{\partial n_q} \right] ds + \int_{S_{RW}} \Delta\phi_{rw}(\vec{x}) \frac{\partial G(p;q)}{\partial n_q} ds$$

Boundary conditions:

1. The flow on the wetted parts of rotor, stator, hub, and casing surfaces should be tangent to the wetted surfaces.

$$\frac{\partial\phi}{\partial n} = \begin{cases} -\vec{V}_{in}\cdot\vec{n} = -\vec{U}_{in}\cdot\vec{n} + (\vec{\varpi}\times\vec{x})\cdot\vec{n}; & \text{on the rotor} \\ -\vec{V}_{in}\cdot\vec{n} = -\vec{U}_{in}\cdot\vec{n} & \text{; on the stator} \end{cases}$$

2. The Kutta condition requires that the fluid velocities at the rotor and stator trailing edge are finite.

$$|\nabla\phi(x,y,z)| < \infty \qquad \text{at rotor or stator trailing edge}$$

An iterative pressure Kutta condition is implemented as described in Kinnas & Hsin (1992).

3. The cavity closure condition implies that the cavity has to be closed at its end. Since the cavity planform is unknown, the boundary value problem is solved at the given cavitation number by using a guessed cavity planform which may not be closed if the pressures on the cavity planform do not correspond to the given cavitation number. The Newton-Raphson iterative method is adopted to find the correct cavity extent which satisfies the cavity closure condition at the given cavitation number (Kinnas & Fine, 1993).

4. The dynamic boundary condition on the cavity surface requires that the pressure on the cavity surface is constant and equal to the constant pressure, p_c, inside the cavity. By manipulating the Bernoulli's equation in the rotating or the fixed coordinate system in terms of the cavitation number, the total velocity, $\vec{q}_t$, on the cavity surface can be given as follows.

$$|\vec{q}_t|^2 = \begin{cases} n^2D^2\sigma_n + |\vec{U}_{in}|^2 + \omega^2r^2 - 2gy_s - 2\dfrac{\partial\phi}{\partial t}; & \text{on rotor} \\ |\vec{U}_{in}|^2(1+\sigma_n) - 2gy_s - 2\dfrac{\partial\phi}{\partial t}; & \text{on stator} \end{cases}$$

where r is the distance from the axis of rotation; g is the gravitational acceleration; y_s is the vertical distance from the horizontal plane through the axis of rotation; n and D are the blade rotational frequency and the rotor diameter, respectively. The cavitation number, σ_n, is defined as follows:

$$\sigma_n = \begin{cases} \dfrac{p_o - p_c}{1/2\rho n^2D^2}_s & \text{for rotor} \\ \dfrac{p_o - p_c}{1/2\rho U_{in}^2} & \text{for stator} \end{cases}$$

where p_o is the pressure far upstream at the depth of the shaft axis, and ρ is the water density.

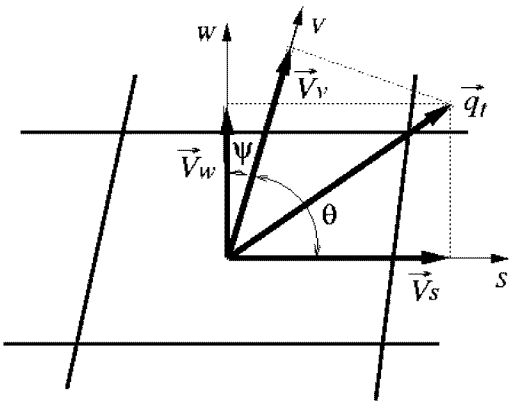

Figure 3: Local coordinates system at each panel. The shown s and v axes are tangent to the blade surface. Axis w is also tangent to the blade surface, and perpendicular to the s axis.

The $-2\partial\phi/\partial t$ term in the Bernoulli equation will be zero in the case of axi-symmetric inflow. Thus, for simplicity, this term will be omitted in the next equations, even though it is still present in the code (where it will also become zero since the inflow is axi-symmetric and $\partial/\partial t = 0$).

The total velocity $\vec{q}_t$ can be expressed in terms of the directional derivatives of the perturbation potential and the inflow components at the non-orthogonal coordinate system:

$$\vec{q}_t = \frac{\left(\dfrac{\partial\phi}{\partial s} + U_s\right)\left[\vec{s} - (\vec{s}\cdot\vec{v})\vec{v}\right] + \left(\dfrac{\partial\phi}{\partial v} + U_v\right)\left[\vec{v} - (\vec{s}\cdot\vec{v})\vec{s}\right]}{\left\|\vec{s}\times\vec{v}\right\|^2} + \left(\frac{\partial\phi}{\partial n} + U_n\right)\vec{n}$$

with $\vec{s}$ and $\vec{v}$ being the unit vectors corresponding to the coordinates s (chordwise) and v (spanwise), respectively, and with $\vec{n}$ being the unit normal vector to the cavity. U_s, U_v, and U_n are the components of the inflow velocity $\vec{V}_{in}$ along the (s,v,n) directions.

Note that: $V_s = \left(\dfrac{\partial\phi}{\partial s} + U_s\right)$, $V_v = \left(\dfrac{\partial\phi}{\partial v} + U_v\right)$, and $V_n = \left(\dfrac{\partial\phi}{\partial n} + U_n\right)$ are the components of the total velocity vector, $\vec{q}_t$, along the directions (s,v,n).

Combining the equations for $|\vec{q}_t|$ and $\vec{q}_t$, given previously, $\dfrac{\partial\phi}{\partial s}$ can be obtained as follows:

$$\frac{\partial \phi}{\partial s} = -U_s + \left(\frac{\partial \phi}{\partial v} + U_v \right) \cos\theta + \sin\theta \sqrt{|\vec{q}_t|^2 - \left(\frac{\partial \phi}{\partial v} + U_v \right)^2}$$

where θ is the angle between $\vec{s}$ and $\vec{v}$, as shown in Figure 3. Note that: $\cos\theta = \vec{s} \cdot \vec{v}$

A Dirichlet type of boundary condition on ϕ is derived by integrating the equation for $\frac{\partial \phi}{\partial s}$:

On the part of the cavity over the blade surface:

$$\phi(s,v) = \phi(0,v) + \int_0^s \left[-U_s + \left(\frac{\partial \phi}{\partial v} + U_v \right) \cos\theta + \sin\theta \sqrt{|\vec{q}_t|^2 - \left(\frac{\partial \phi}{\partial v} + U_v \right)^2} \right] ds$$

and, on the part of the cavity over the wake surface is:

$$\phi^+(s,u) = \phi(s_{TE},u) + \int_{s_{TE}}^s \left[-U_s + \sqrt{|\vec{q}_t|^2 - \left(\frac{\partial \phi^+}{\partial u} + U_u^+ \right)^2} \right] ds$$

The potential $\phi(0,v)$ corresponds to the potential value at the cavity leading edge, and can be extrapolated in terms of the unknown potentials of wetted flow panels in front of the cavity detachment location. $s = s_{TE}$ denotes the blade trailing edge. The variable u in the equation for $\phi^+(s,u)$ corresponds to the directional derivative normal to (s,n) plane on wake surface, and the superscript, +, represents the upper side of the wake sheet. The equation for the potential on the cavity includes the unknown functions, $\frac{\partial \phi}{\partial v}$ and those terms are determined in an iterative manner.

5. The kinematic boundary condition on cavity surface requires that the substantial derivative of the cavity surface has to vanish. Once the boundary value problem is solved, the kinematic condition is utilized to determine the position of the cavity surface.

$$\left(\frac{\partial}{\partial t} + \vec{q}_t \cdot \nabla \right) \left[n - h(s,v) \right] = 0$$

where $h(s,v)$ is the cavity thickness normal to the blade surface.

By substituting the gradient in terms of the local directional derivatives, the partial differential equation for the cavity thickness is derived as follows:

$$\frac{\partial h}{\partial s}\left[V_s - \sin\theta \cdot V_v \right] + \frac{\partial h}{\partial v}\left[V_v - \sin\theta \cdot V_s \right] = V_n \cos^2\theta$$

Where

$$V_s = \frac{\partial \phi}{\partial s} + U_s, \qquad V_v = \frac{\partial \phi}{\partial v} + U_v, \qquad V_n = \frac{\partial \phi}{\partial n} + U_n$$

The cavity height normal to the blade surface can be determined by solving the above partial differential equation which includes the solution $\frac{\partial \phi}{\partial n}$ of the integral equation for the rotor and stator.

The cavity height on wake surface, (h_w), when the super-cavity occurs, is similarly determined in terms of the cavity source on the wake surface:

$$\frac{\partial h_w}{\partial s} |\vec{q}_t| = \frac{\partial \phi^+}{\partial n} - \frac{\partial \phi^-}{\partial n}$$

6. The cavity detachment location on either side of the blade is determined iteratively to satisfy the *smooth detachment condition* as described in Young and Kinnas (2001). The cavity detachment may also be determined via coupling with XFOIL (Drela, 1989) as described in Brewer & Kinnas (1997) and Sun & Kinnas (2006).

7. The velocity at the inlet has to be equal to that specified, i.e. $\vec{q} = \vec{V}_{in}$, and that leads to the Neumann type of condition at the inlet:

$$\left. \frac{\partial \phi}{\partial n} \right|_{in} = 0 \text{ at the inlet}$$

Similarly, at the outlet we should have:

$$\left. \frac{\partial \phi}{\partial n} \right|_{out} = (\vec{q}_{out} - \vec{q}_{in}) \cdot \vec{n}$$

If U_{out} is the axial component of $\vec{q}_{out}$ we get:

$$\left. \frac{\partial \phi}{\partial n} \right|_{out} = U_{in} - U_{out} \text{ at the outlet}$$

Assuming that U_{out} is uniform[1], we can determine its value from applying continuity:

$$U_{in} \cdot A_{in} = U_{out} \cdot A_{out} \Rightarrow U_{out} = U_{in} \frac{A_{in}}{A_{out}}$$

where A_{in} and A_{out} are the casing areas at the inlet and outlet.

Interaction between rotor and stator:

The fluid field around the waterjet propulsor is solved in an iterative manner by solving the integral equations for rotor and stator separately and by considering the

[1] As shown in Choi & Kinnas (1998) this assumption has negligible effect on the flow around the propeller.

effect of each component on the other by using the induced potentials from one to the other. The induced potentials on the other component are calculated using the integral equation for $4\pi\phi_{RS}(\vec{x})$ and $4\pi\phi_{SR}(\vec{x})$, and are circumferentially averaged to apply on the control points. The problems for both components are iterated until the forces converge within a certain criterion. Figure 4 shows how the induced potentials due to the rotor are included at the control point on the stator, and the averaged potentials on the stator induced by each panel on the key blade of the rotor can be derived as follows (N is the number of equally spaced elements over an angle equal to the angle between two rotor blades):

$$\phi_{SR}^{1} = \frac{\sum_{i=1}^{i=N} \phi_i^1}{N}$$

Finally, it should be noted that the swirl (tangential velocity) induced by the rotor on the stator (assumed to be post-swirl) will also need to be evaluated (by averaging circumferentially the tangential velocity with respect to the angular position) and then included, as a velocity term, in the kinematic boundary condition on the stator blades. Thus the kinematic boundary condition on the stator blades must be adjusted as follows:

$$\left.\frac{\partial\phi}{\partial n}\right|_{stator} = -(\vec{U}_{in} + \vec{u}_{\tan,SR})\cdot\vec{n}$$

where $\vec{u}_{\tan,SR}$ is the tangential (swirl) velocity induced by the rotor on the stator control points. Please note that this adjustment is not required for the kinematic boundary condition on the rotor, since the stator does not induce any (circumferentially averaged) swirl upstream of it.

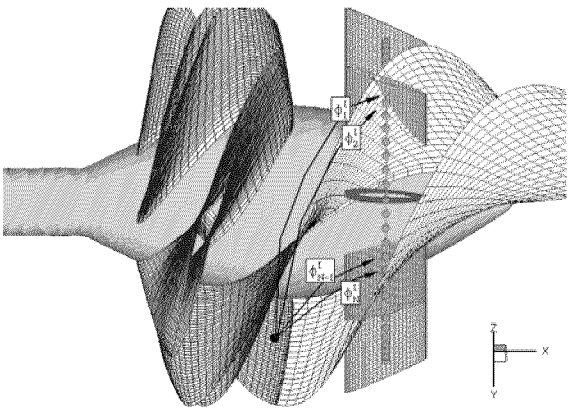

Figure 4: Schematic showing the inclusion of the circumferentially averaged rotor effects on the stator control points

Numerical Implementation

A constant dipole and source panel method (code name PROPCAV) is utilized in order to solve either the rotor or the stator problem. Representative panel arrangements on the various components of a notional waterjet pump are shown in Figures 5-7. The panels for the rotor or the stator problems are aligned with the geometry at the tip of the rotor or the stator blades, respectively, as shown in Figures 6 and 7. Special care has to be taken with the panel arrangement at the junctions of the blades with the hub or the casing, as shown in Figure 8, in order to avoid highly distorted panels.

It should be noted that, at this stage, we assume that the tip gap of the rotor is equal to zero, even though the actual gap is usually under 1%. As shown in Kerwin (2006), where the orifice equation was implemented in the case of a wing close to a wall, for a gap of 1% the results with zero gap were much closer to those from inviscid theory with the orifice equation implemented, than to those from inviscid theory where the actual gap was used.

The results are represented in a non-dimensional manner, as follows:

$$J = \frac{U_{in}}{n\ D} \quad \text{the advance ratio}$$

$$K_T = \frac{T}{\rho n^2 D^4} \quad \text{the thrust coefficient}$$

$$K_Q = \frac{Q}{\rho n^2 D^5} \quad \text{the torque coefficient}$$

$$C_P = \frac{p - p_o}{1/2\rho n^2 D^2} \quad \text{the pressure coefficient (for rotor or stator)}$$

$$G = \frac{100 * \Delta\phi_{TE}}{\pi D U_{ref}} \quad \text{the circulation distribution (for rotor or stator)}$$

Where T and Q are the thrust and torque, respectively, acting on the rotor, D and n are the rotor diameter and rotational frequency, $\Delta\phi_{TE}$ the potential jump at the trailing edge of the rotor or stator blade, and U_{ref} is the reference velocity defined as:

$$U_{ref} = \sqrt{U_{in}^2 + (0.7\pi nD)^2}$$

In the case of cavitation the pressure on the cavity should be equal to the vapor pressure and, according to the definition of the cavitation number for the rotor, the following equation should be valid on the cavity:

$$-C_P = \sigma_n$$

In the case of pumps it is also customary to evaluate the headrise (rise in total pressure head) from the inlet and outlet section. The authors plan to evaluate this headrise within the context of their method in the very near future.

VERIFICATION AND VALIDATION

Results and grid dependence studies in wetted and cavitating flow

To study the numerical performance of the current model the method is first applied on a notional waterjet pump, which is based on the one which is currently being tested at Johns Hopkins University with support by the Office of Naval Research.

The results from several grid dependence studies are presented in Figures 9-19. Figures 9 and 10 show the effect of the stator on the rotor as the number of iterations between the two increases. Note that the iterative process converges very quickly, within the 1st iteration in this case (the 0th iteration corresponds to the rotor solution without the stator). Figure 11 shows the effect of the stator on the predicted thrust and torque on the rotor. Figure 12 shows the convergence of the predicted circulation distribution on the rotor with number of panels on the rotor. Figures 13 and 14 show the convergence of the predicted circulation distribution (wetted and cavitating) with the number of panels between the blades in the circumferential direction. Figure 15 shows the convergence of the wetted circulation distribution with the size of the increment in the rotational direction, $\Delta\theta$, which sets the size of the panels in the axial direction on the trailing wake of the rotor as well as on the hub and casing. Figures 16 and 17 show the wetted and cavitating pressure distributions at different sections along the span of the rotor blades. Please note that the cavitating pressure distributions are such that $-C_P = \sigma_n$ on the cavity and $-C_P < \sigma_n$ everywhere else on the blade. Figures 18 and 19 show contour plots and the predicted cavities on both sides of the rotor blades. It should be noted that midchord back and leading edge face cavities are predicted in this case.

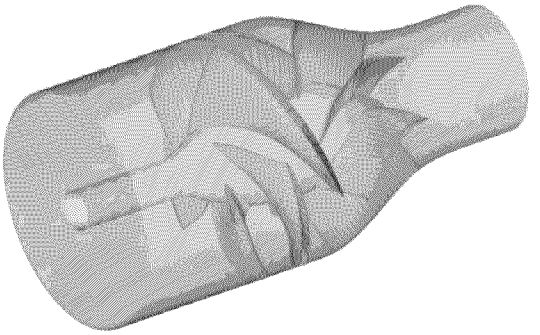

Figure 5: Paneled geometry of a notional waterjet pump with a 5-blade rotor and a 7-blade stator. Viewed from upstream.

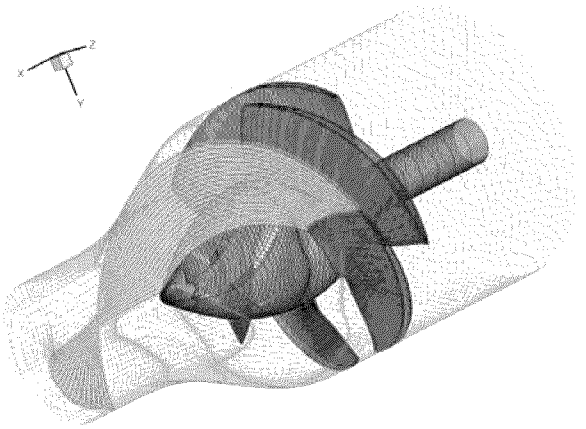

Figure 6: Paneled geometry of a notional waterjet pump for the rotor problem (the trailing wake of one blade is also shown). Viewed from downstream.

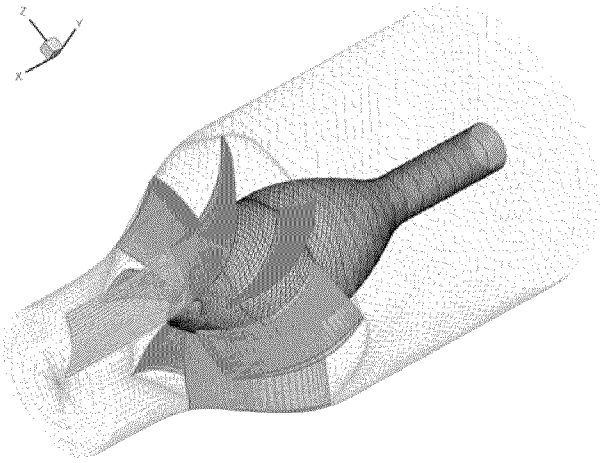

Figure 7: Paneled geometry of a notional waterjet pump for the stator problem (the trailing wake of one blade is also shown). Viewed from downstream.

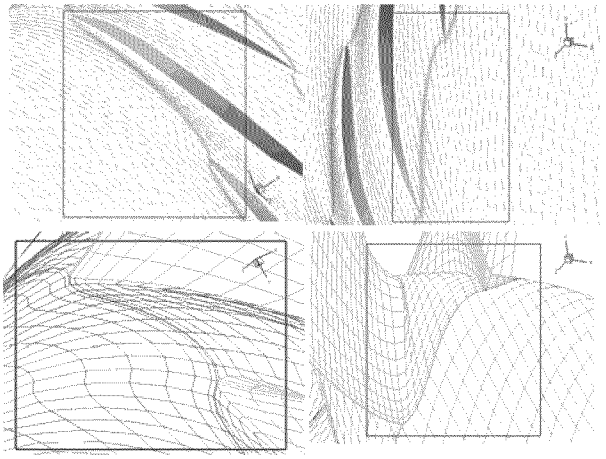

Figure 8: Details of paneling: on the casing at the blade leading edge (top left), on the casing at the blade trailing edge (top right), on the hub at the blade leading edge (bottom left), and on the hub at the blade trailing edge (bottom right).

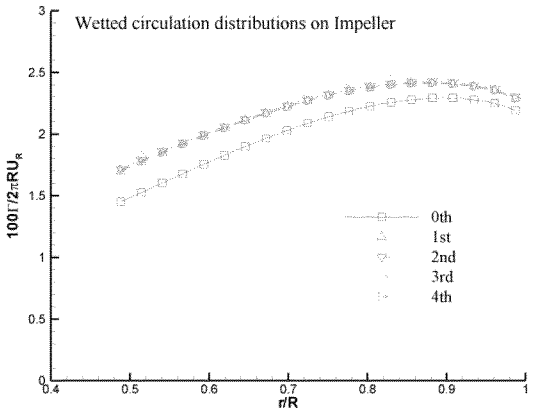

Figure 9: Convergence of wetted circulation distribution on rotor with number of iterations for a notional waterjet pump at J=0.6 (the 0^{th} iteration corresponds to the rotor solution without the stator)

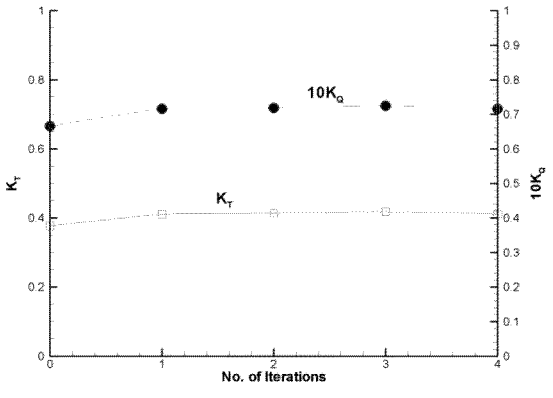

Figure 10: Convergence of rotor (wetted) thrust and torque with number of iterations between rotor and stator for a notional waterjet pump at J=0.6 (the 0^{th} iteration corresponds to the rotor solution without the stator).

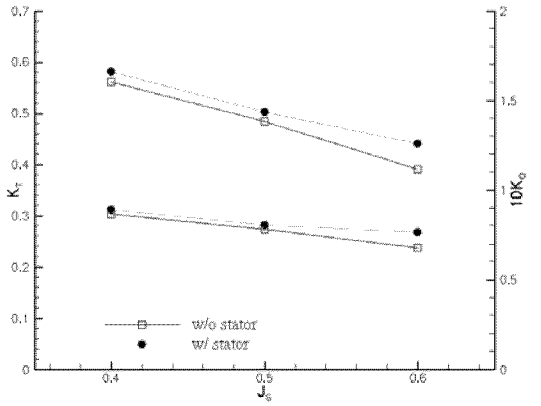

Figure 11: Predicted rotor thrust and torque coefficients with and without including the influence of the stator for the notional waterjet pump at $\sigma_n = 1.0$

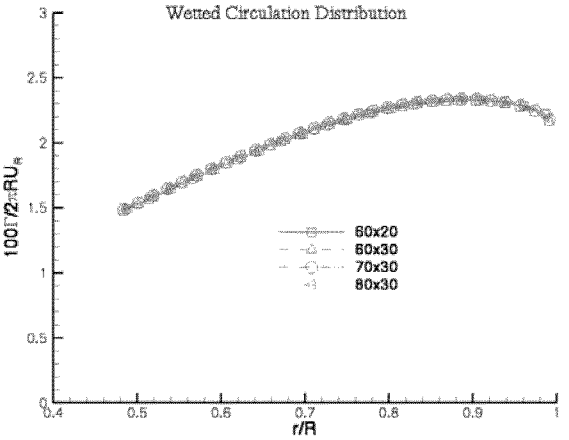

Figure 12: Convergence of the predicted wetted circulation distribution with number of panels on the rotor blade for the notional waterjet pump at J=0.6

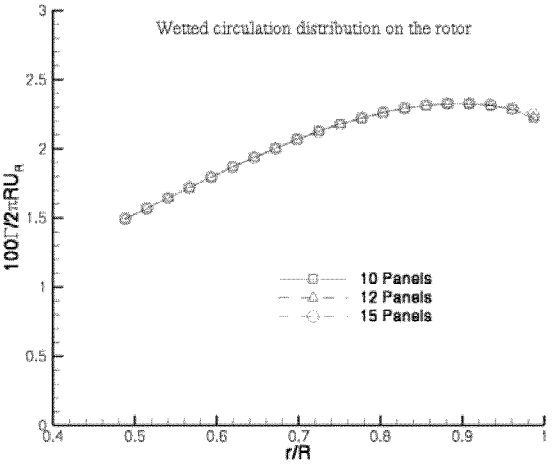

Figure 13: Convergence of the predicted wetted circulation distribution with the number of panels in the circumferential direction between the blades for the notional waterjet pump at J=0.6

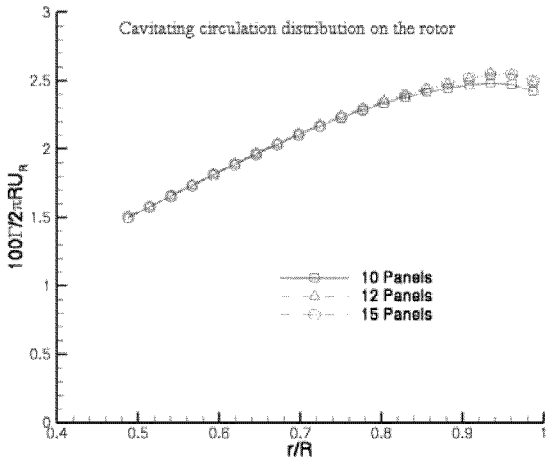

Figure 14: Convergence of the predicted cavitating circulation distribution with the number of panels in the circumferential direction between the blades for the notional waterjet pump at J=0.6 and $\sigma_n = 1.0$

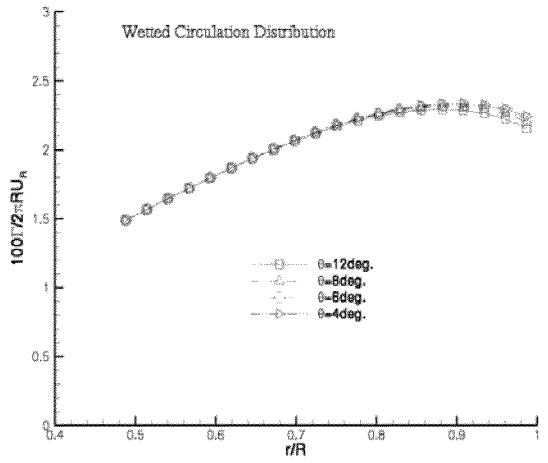

Figure 15: Convergence of the predicted wetted circulation distribution on the rotor with panel size in the wake, $\Delta\theta$, for the notional waterjet pump at J=0.6 and $\sigma_n = 1.0$

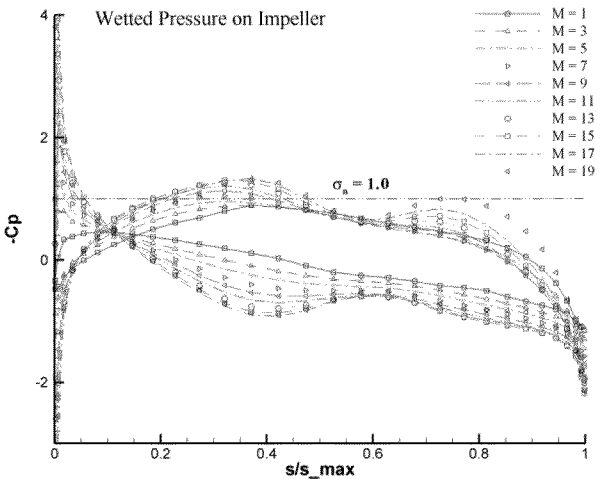

Figure 16: Predicted wetted pressure distributions on the rotor for the notional waterjet pump at J=0.6.

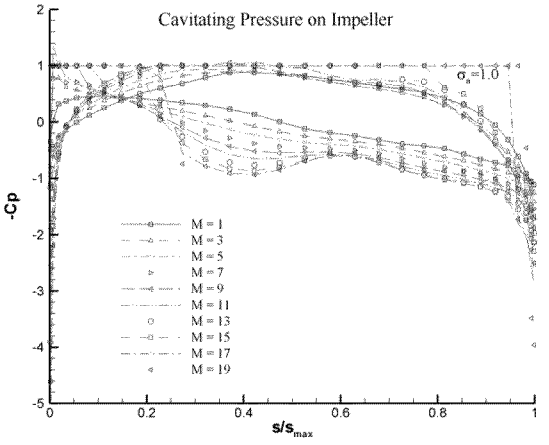

Figure 17: Predicted cavitating pressure distributions on the rotor for the notional waterjet pump at J=0.6 and $\sigma_n = 1.0$.

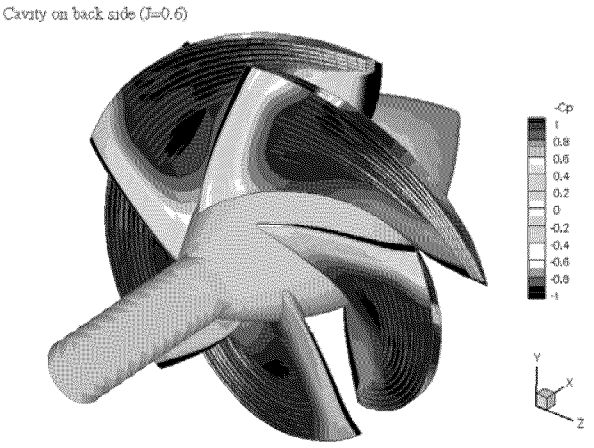

Figure 18: Contour plots of predicted pressures and cavity patterns on the suction side (back) of the rotor blades; notional waterjet pump at J=0.6 and $\sigma_n = 1.0$, view from upstream.

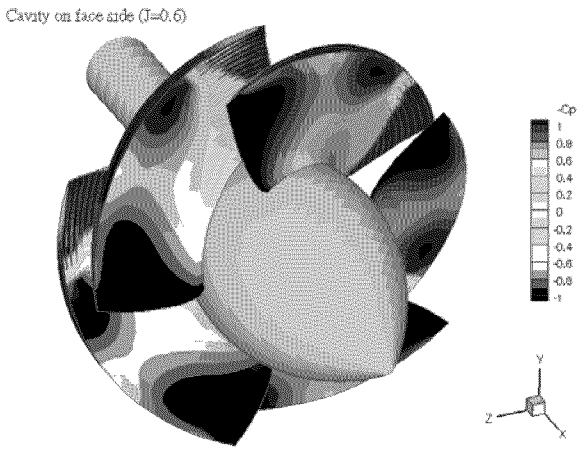

Figure 19: Contour plots of predicted pressure distributions and cavity patterns on pressure side (face) of the rotor blades; notional waterjet pump at J=0.6 and $\sigma_n = 1.0$, view from downstream.

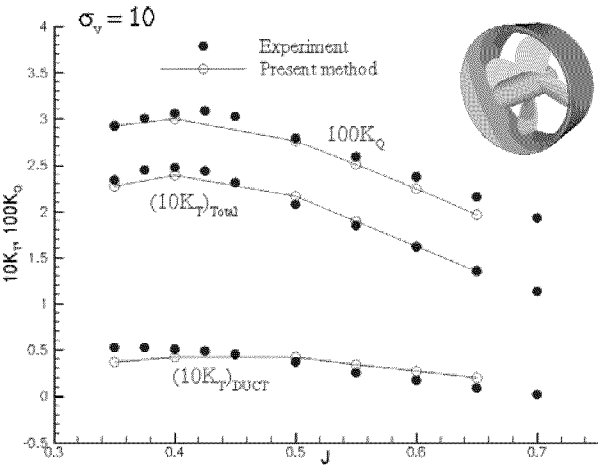

Figure 21: Thrust and torque break-down due to cavitation, predicted by the present method when applied on the P1452 propeller inside the D15 duct, and measured by Dyne (1973) (From Lee and Kinnas, 2006)

Validation for ducted propellers

Some correlations of the present method when applied to ducted propellers, are presented in Figures 20 and 21. Please note the appreciable effects of viscosity on the predicted propeller torque shown in Figure 20. Figure 21 shows the effect of cavitation on thrust and torque breakdown.

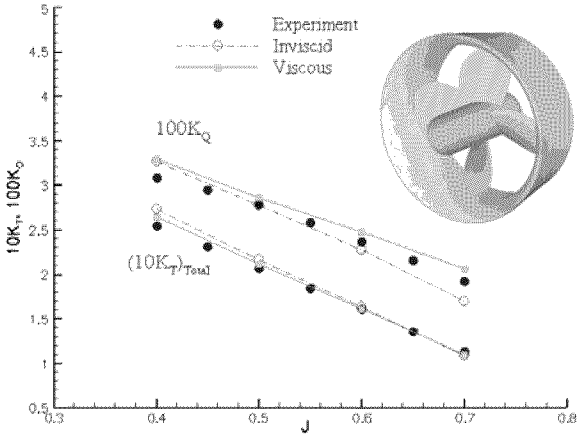

Fig.20: Comparison of the measured and predicted blade forces with measured on P1452 propeller and D15 duct (Dyne, 1973). The viscous results have been produced via interactive coupling of the present method with XFOIL on the propeller blades (from Kinnas et al, 2007)

Application to the CCDoTT waterjet pump

The method was then applied on a waterjet designed by CCDoTT (Center for the Commercial Deployment of Transportation Technologies) of California State University, Long Beach, and developed in conjunction with CDI Marine. A side view of the waterjet is shown in Fig. 22 and its main characteristics are given in Table 1. The CCDoTT waterjet was tested in the 24-inch water tunnel at the David Taylor Model Basin at NSWCCD as reported by Brewton et al (2006), who also made calculations using the commercial RANS solver Fluent.

The paneling on the rotor and stator blades, the hub and the casing are shown in Figure 23. The predicted pressures on the rotor and stator blades at design flow rate are shown in Figures 24-26. Finally, the predicted vs. measured torque on the rotor blades is shown in Figure 27. Note that the predicted torque is lower than measured even at the design flow rate. The authors think that due to the rounded trailing edge of the rotor blades the effects of viscosity might be significant, but at this stage the effects of viscosity on the torque were evaluated by just applying a uniform friction coefficient on the blades. In addition the authors assumed a zero gap at the rotor tip even though the actual gap is about 0.5% of the rotor radius. Thus, the effects of the viscous gap flow and of the associated tip gap vortex on the solution were not accounted for properly.

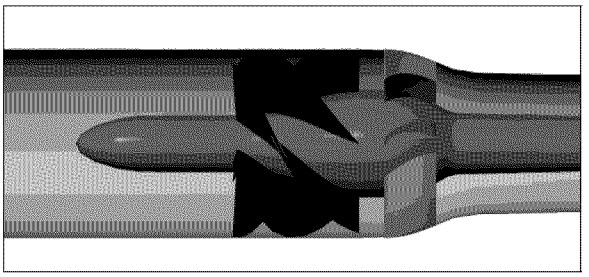

Figure 22: A side view of the CCDoTT waterjet in its shroud (from Brewton et al, 2006)

Casing Diameter	0.1905 m
Rotor Diameter	0.1895 m
Rotor Blades	5
Stator Blades	8
Impeller Chord Length	0.1516 m
Stator Chord Length	0.07389 m
Rotor Hub Diameters	0.0572 m (forward); 0.109 m (rear)
Stator Hub Diameters	0.109 m (forward); 0.0508 m (rear shaft)
Rotational Speed	1700 rpm
Mass Flow at Design	164.681 kg/s

Table 1: Specifications for CCDoTT pump geometry (from Brewton et al, 2006)

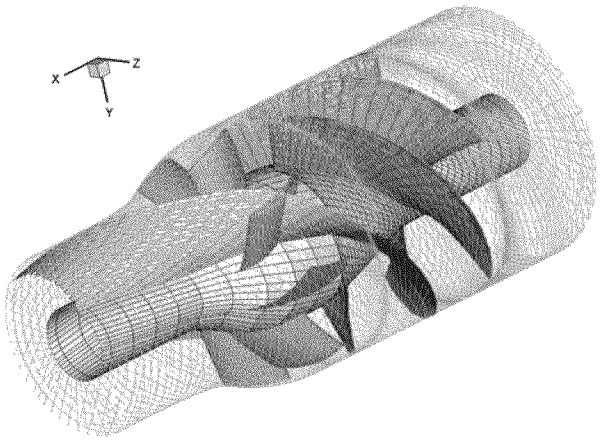

Figure 23: The paneling on the CCDoTT waterjet. The trailing wake of one of the rotor blades is also shown.

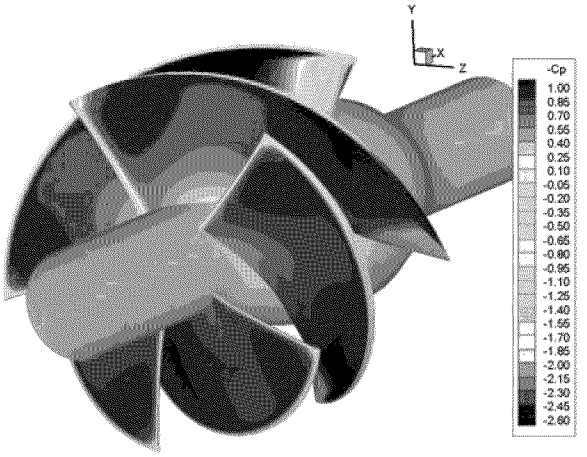

Figure 24: Predicted pressures on suction side (back) of rotor blades for CCDoTT waterjet at design flow rate. Viewed from upstream.

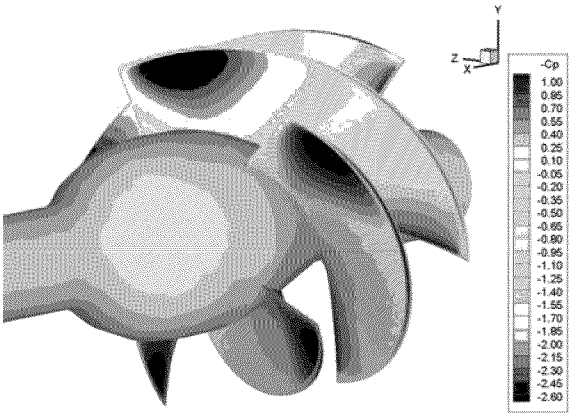

Figure 25 : Predicted pressures on pressure side (face) of rotor blades for CCDoTT waterjet at design flow rate. Viewed from downstream.

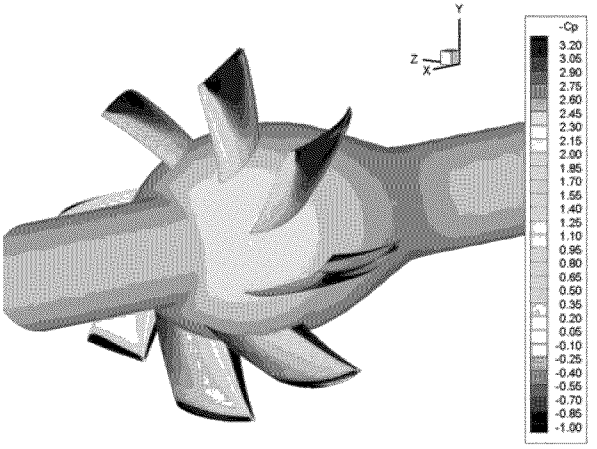

Figure 26: Predicted pressures on stator blades for CCDoTT watejet at design flow rate. Viewed from downstream.

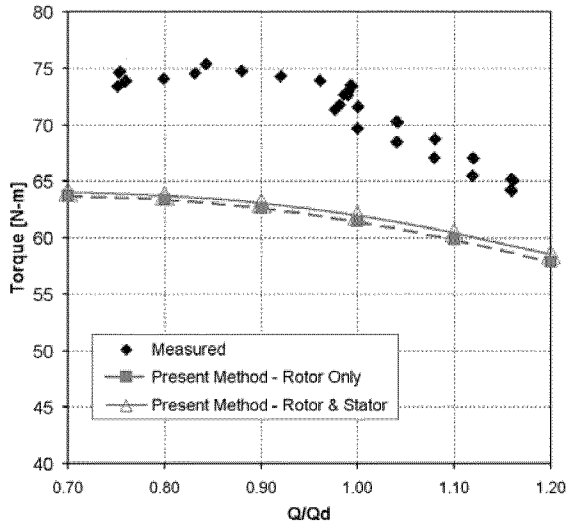

Figure 27: Predicted by the present method and measured torque for the CCDoTT waterjet versus the ratio of the flow rate to the design flow-rate.

CONCLUSIONS

A boundary element method was extended to predict the performance of waterjet pumps subject to uniform inflow, including the effects of sheet cavitation. The interaction between the rotor and the stator was evaluated in an iterative manner, by considering the circumferentially averaged effects of one on the other.

Preliminary predictions of the torque on a previously tested waterjet were found to be lower than those measured. The discrepancy between the predictions and the measurements might be attributed to the effects of viscosity on the blade pressures and torque in the case of round trailing edge sections, as well as to the effects of the viscous gap flow on the rotor performance.

The authors intend to include the effects of viscosity on the rotor blades of waterjets by extending the method of Sun & Kinnas (2006). They also plan on including the effects of the viscous tip gap on waterjet rotors by applying the orifice equation approach (Kerwin et al, 1987), as was recently implemented in the case of ducted propellers by Kinnas et al (2004), as well as by tracking the tip gap vortex and its effect on the blade loading by applying the method presented in Gu (2006). Systematic correlations with the detailed flow field velocity and pressure measurements, to be reported from the waterjet tests which are being performed at Johns Hopkins University, will also be carried out.

Future challenges include the application of the method to cavitating waterjets (e.g. correlation of predicted to observed cavity planforms on rotor or stator blades and prediction of rotor thrust and torque breakdown due to cavitation), and the prediction of the unsteady cavitating performance of waterjets. The latter task will allow for the prediction of the performance of waterjets which are often subject to non-axisymmetric inflows (due to the wakes of the waterjet components upstream of the rotor), and will involve the evaluation of the 3-D (time-averaged or unsteady) effective wake to the rotor or stator blades via coupling with a method (e.g. a RANS solver) which solves for the global flow inside the waterjet including at least the inlet, the outlet, as well as a part of the hull in the vicinity of the waterjet.

ACKNOWLEDGMENTS

Support for this research was provided by the U.S. Office of Naval Research (Contract N00014-07-1-0616) and Phases IV and V of the "Consortium on Cavitation Performance of High Speed Propulsors" with the following current members: American Bureau of Shipping, Daewoo Shipbuilding and Marine Engineering Co. Ltd., Kawasaki Heavy Industry Ltd., Rolls-Royce Marine AB, Rolls-Royce Marine AS, Samsung Heavy Industries Co. Ltd., VA Tech Escher Wyss GmbH, Wärtsilä Propulsion Netherlands B.V., Wärtsilä Propulsion Norway AS, Wärtsilä Lips Defense S.A.S., and Wärtsilä CME Zhenjiang Propeller Co. Ltd.

The authors wish to thank Dr. Ki-Han Kim for his continuing support and encouragement of this work through the U.S. Office of Naval Research.

The authors would also like to thank CDI Marine for making the detailed pump geometry available in order to perform the simulations.

REFERENCES

Brewer, W.H. and Kinnas, S.A., "Experiment and Viscous Flow Analysis on a Partially Cavitating Hydrofoil ," *Journal of Ship Research*, Vol. 41, pp. 161-171, 1997.

Brewton, S., Gowing, S., and Gorski S. "Performance Predictions of a Waterjet Rotor and Rotor/Stator Combination Using RANS Calculations", *Twenty-sixth Symposium on Naval Hydrodynamics,* Rome, Italy, September 17-22, 2006

Choi, J.-K. and Kinnas, S.A., "Numerical Water Tunnel in Two and Three Dimensions," *Journal of Ship Research*, Vol. 42, pp. 86-98, 1998.

Chun, H.H., Park, W.G., and Jun, J.G. Experimental and CFD Analysis for Rotor-Stator Interaction of a Waterjet Pump. In Proceedings of the 24th Symposium on Naval Hydrodynamics, Fukuoka, Japan, July 2002.

Drela, M. "XFOIL: An Analysis and Design System for Low Reynolds Number Airfoils," Lecture Notes in Engineering (Vol. 54, Low Reynolds Number Aerodynamics), New-York, Springer-Verlag, 1989.

Gu, H., "Numerical Modeling of Flow around Ducted Propellers," PhD Thesis, Department of Civil Engineering, The University of Texas at Austin, August, 2006.

Kerwin, J.E., Kinnas, S.A., Lee, J.-T. and Shih, W.-Z., "A Surface Panel Method for the Analysis of Ducted Propellers," *Trans. SNAME*, Vol. 95, pp. 93-122, 1987

Kerwin, J.E., Michael, T.J. and Neely, S.K. "Improved Algorithms for the Design/Analysis of Multi-Component Complex Propulsors ". In 11th Propellers/Shafting Symposium, Williamsburg, Virginia, September 2006.Society of Naval Architects and Marine Engineers

Kerwin, J.K. "Hydrodynamic Issues in Waterjet Design and Analysis", *Twenty-sixth Symposium on Naval Hydrodynamics,* Rome, Italy, September 17-22, 2006.

Kinnas, S.A. and Fine, N.E., "A Nonlinear Boundary Element Method for the Analysis of Unsteady Propeller Sheet Cavitation," Proceedings of *Nineteenth Symposium on Naval Hydrodynamics,* Office of Naval Research, National Academy Press, pp. 717-737, 1992.

Kinnas, S.A. and Hsin, C.-Y., "Boundary Element Method for the Analysis of the Unsteady Flow Around Extreme Propeller Geometries," *AIAA Journal*, Vol. 30, pp. 688-696, 1992.

Kinnas, S.A. and Fine, N.E., "A Numerical Nonlinear Analysis of the Flow Around 2-D and 3-D Partially Cavitating Hydrofoils," *Journal of Fluid Mechanics*, Vol. 254, pp. 151-181, 1993.

Kinnas, S.A., Choi, J.-K., Lee, H., Young, Y.L., Gu, H., Kakar, K. and Natarajan, S., "Prediction of Cavitation Performance of Single or Multi-component Propulsors and their Interaction with the Hull," *Trans. Society of Naval Architects and Marine Engineers*, Vol. 110, pp. 215-244, 2002.

Kinnas, S.A. and Lee, H., and Gu, H., and Gupta, A." Prediction of Performance of Ducted and Podded Propellers," *25th Symposium on Naval Hydrodynamics,* August 8-13, 2004, St. John's, Newfoundland and Labrador, Canada.

Kinnas, S. A. and Lee, H. S. and Gu, H. and Deng, Y., "Prediction of Performance and Design via Optimization of Ducted Propellers subject to Non-axisymmetric Inflows," Trans. of The Society of Naval Architects & Marine Engineers, Vol. 113, 2005, pp. 99-121.

Kinnas, S.A., Lee, H., Gu, H., and Natarajan, S. "Prediction of sheet cavitation on a rudder subject to propeller flow," *Journal of Ship Research,* Vol. 51, pp. 65-75, March 2007.

Kinnas, S.A., Lee, H.S., Sun, H., and He, L. "Performance Prediction of Single and Multi-component Propulsors using Coupled Viscous/Inviscid Methods," PRADS'07, Houston, TX, October 1-5, 2007.

Lee, H., *Modeling of Unsteady Wake Alignment and Developed Tip Vortex Cavitation*, PhD thesis, UT Austin, Ocean Engineering Group, Department of Civil Engineering, August 2002 (also UT-OE Report 02-4)

Lee, H. and Kinnas, S.A., "Application of BEM in the Prediction of Unsteady Blade Sheet and Developed Tip Vortex Cavitation on Marine Propellers," *Journal of Ship Research*, Vol. 48, No. 1, pp. 15-30, March 2004.

Lee, H. and Kinnas, S.A., "Fully Unsteady Wake Alignment for Propellers in Non-axisymmetric Flows," *Journal of Ship Research*, Vol. 49, No. 3, pp. 176-190, September 2005.

Lee, H. S. and Kinnas, S. A., "A BEM for the Modeling of Unsteady Propeller Sheet Cavitation inside a Cavitation Tunnel," Journal of Computational Mechanics, Vol.37, No. 1, 2005, pp.41-51.

Lee, H. S. and Kinnas, S. A., "Prediction of Cavitating Performance of Ducted Propeller," Sixth International Symposium on Cavitation, September 11-15, 2006, Wageningen, The Netherlands.

Sun, H. and Kinnas, S. A." Simulation of sheet cavitation on propulsor blades using a viscous/inviscid interactive method", in *CAV2006*: Sixth International

Symposium on Cavitation, Wageningen, The Netherlands, September 11-15, 2006

Taylor, T.E., Scherer, J.O., and Kerwin, J.E."Waterjet Pump Design and Analysis Using a Coupled Lifting-Surface and RANS Procedure". In Royal Institution of Naval Architects Conference on Waterjet Propulsion – Latest Developments, Amsterdam, The Netherlands, 1998.

Young, Y.L. and Kinnas, S.A., "A BEM for the Prediction of Unsteady Midchord Face and/or Back Propeller Cavitation," *Journal of Fluids Engineering*, Vol. 123, pp. 311-319, June 2001

Young, Y.L., *Numerical Modeling of Supercavitating and Surface-Piercing Propellers*, PhD thesis, UT Austin, Ocean Engineering Group, Department of Civil Engineering, May 2002 (also UT-OE Report 02-1)

Young, Y.L. and Kinnas, S.A., "Numerical Modeling of Supercavitating Propeller Flows," *Journal of Ship Research*, Vol. 47, pp. 48-62, March 2003.

Young, Y.L. and Kinnas, S.A., "Performance Prediction of Surface-Piercing Propellers," *Journal of Ship Research*, 2004, Vol. 48, No. 4, pp. 288-304, December 2004.

DISCUSSIONS AND AUTHOR'S REPLIES

NAME OF DISCUSSER:
Henk de Koning Gans

QUESTION:
The wake of the rotor intersects the stator so a small slice of the wake is inside the stator. The question now is: has the slice of the wake inside the stator influenced the boundary condition at the stator collocation point? And has, therefore, the inner slice of wake to be subtracted?

AUTHOR'S REPLY:
In the present work the circumferentially averaged (or time averaged) effect of the rotor wake on the stator is considered. Thus, excluding the wake elements which are inside the stator blade, should have a negligible effect on the circumferentially averaged values. In the following paper by Kinnas et al, where the interaction between a propeller tip vortex and a rudder was addressed in an *unsteady* manner, the vortex looped around the leading edge of the rudder, and was not allowed to intersect it.

Kinnas, S.A., Mohhamed, F., and Lee, H. "Propeller Tip Vortex/Rudder Interaction", *Twenty-sixth Symposium on Naval Hydrodynamics*,, September 2006, Rome, Italy.

NAME OF DISCUSSER:
Ki-Han Kim

QUESTION:
Where did you apply the Kuttta condition for the blade with a round trailing edge? The effect of the location of Kutta condition application on the K_T and K_Q for a round trailing edge would be significant.

AUTHOR'S REPLY:
In this paper, the application of Kutta condition to a round trailing edge blade is not addressed. Instead, the round trailing edge is modified to be a sharp one by reducing the blade thickness, and an iterative pressure Kutta condition is applied at the sharp trailing edge. The authors agree with Dr. Kim that in the case of a round trailing edge the location where the Kutta condition is applied can have a significant effect on the circulation distribution, and thus on the predicted thrust and torque. However, once the inviscid solution is coupled with the boundary layer solver, the effect of the location of the application of the Kutta condition on the final viscous solution should be less significant.

NAME OF DISCUSSER:
M. Kinzel

QUESTION:
In XFOIL, do you allow the boundary layers to develop over the cavity or do you allow a slip or zero shear stress condition?

AUTHOR'S REPLY:
For sheet cavitation, the water/vapor interface is treated as a constant pressure (free) streamline. The boundary layers are allowed to develop over the cavity surface by setting zero shear stress on the top of the cavity surface, i.e. by forcing the friction coefficient C_f to be 0.

NAME OF DISCUSSER:
J. Young

QUESTION:
Is the presence of the stator accounted for in the wake alignment with the rotor, and visa versa?

AUTHOR'S REPLY:
In the results presented in this paper, there was no wake alignment performed, and the rotor and stator wakes were set at the same pitch as the corresponding blade pitch.